Proceedings of Global Power and Propulsion Society
ISSN-Nr: 2504-4400
GPPS Hong Kong 2023
October 17-19, 2023
www.gpps.global

GPPS-TC-2023-0220

A RAPID PREDICTION METHOD OF BROADBAND NOISE OF SINGLE-STAGE FANS

Xinyu Zhao
Turbomachinery Aerodynamics and Acoustics Lab (TAAL), School of Power and Energy,Northwestern Polytechnical University
xinyuzhao@mail.nwpu.edu.cn
Xi'an Shaanxi, P.R.China

Hang Tong
Turbomachinery Aerodynamics and Acoustics Lab (TAAL), School of Power and Energy,Northwestern Polytechnical University
tonghang@mail.nwpu.edu.cn
Xi'an Shaanxi, P.R.China

Weiyang Qiao
Turbomachinery Aerodynamics and Acoustics Lab (TAAL), School of Power and Energy,Northwestern Polytechnical University
qiaowy@nwpu.edu.cnl
Xi'an Shaanxi, P.R.China

ABSTRACT

A fast broadband noise prediction method was developed for the fan. The main purpose is to quickly obtain the broadband noise spectrum and characteristics of the fan after obtaining the aerodynamic characteristics. The broadband noise model of the fan in this paper is a semi-analytical model based on the steady Reynolds Average Navier-Stokes equation (RANS), which extracts the upstream blade wake turbulence information of the sound source through the steady Computational Fluid Dynamics (CFD) calculation results, and then couples the turbulence information with the analytical model to quickly predict the fan broadband noise level. In this paper, the established fast broadband noise prediction model is introduced, and then, the analytical method part of the broadband noise model is verified by the experimental data of an annular cascade acoustic experimental platform. Finally, the predicted and evaluated aerodynamic performance and acoustic performance of a single-stage axial fan is carried out by using the established fast broadband noise prediction model. The results show that the distribution of upstream turbulence of the sound source is directly related to the secondary flow of the upstream blades. In addition, when the actual operating state of the fan deviates from the design operating state, the level of broadband noise increases significantly, the sound power level (PWL) of broadband noise increases by up to about 5 dB above 5 kHz for NPU-Fan.

Keywords: fan; aeroacoustics; duct acoustics; broadband noise; semi-analytic method

INTRODUCTION

With the rapid development of the world economy and the international commercial air transport market, the noise pollution of commercial aircraft has been paid more and more attention by the whole society(ENGHARDT L,2019).

Engine noise has always occupied a dominant position in aircraft noise(OWENS R,1979).In the past decades, the use of commercial aircraft engines with high bypass ratios has resulted in significant reductions in nozzle exit velocity and effective control of engine jet noise. However, the increase in engine bypass ratio increases the fan size and fan tip speed, making the engine fan noise another significant noise source(HUGHES C,2013).Therefore, fan noise reduction is imminent.

Fan noise can generally be divided into two categories: Fan rotor/stator interaction tone noise(WANG L F,2017;TONG H,2020; TONG H,2021) and Fan Broadband Noise(TONG F,2018; POLACSEK C,2015; TONG H et al,2021). With the

development of computer technology, techniques for predicting fan rotor/stator interaction tone noise have been developed and matured. It is possible to match the noise prediction time with the aerodynamic design time for the rotor/stator interaction tone noise of fan . However, due to the complexity of fan broadband noise, its prediction techniques have been slow to develop and require significant time cost and computational resources. With the effective control of rotor/stator interaction tone noise(Edmane Envia,2002), the engineering problem of fan broadband noise is highlighted, which has become a major problem for civil aviation. (YAN Q ea al,2022).

For the prediction of fan broadband noise, if CFD software is to be used to accurately simulate the rotor wake turbulence and stator interaction process, it is necessary to use Delayed Detached Eddy Simulation (DDES)(CHEN H et al,2023), Large Eddy Simulation (LES) (SHI F C et al,2023)or even Direct Numerical Simulation (DNS).This is still an expensive task even for today's computational resources. In the last decade, semi-analytical models based on the steady Reynolds Average Navier-Stokes (RANS) equations have been introduced (TONG H ea al,2021; Ju H B ea al,2015; Ju H B,2016), which use the rotor wake turbulence information calculated by the RANS method as input, and then use the analytical model to quickly predict the broadband noise. In general, this method can simulate the stator leading edge turbulence information more accurately and promptly, taking into account the characteristics of the analytical model calculations, hence it's use to predict the broadband noise of the fan in the three-dimensional design stage is reasonable.

A RANS turbulence semi-analytical model is developed to predict the wide-band noise of a fan. The RANS turbulence model is validated by experimental data. Furthermore, a single-stage axial fan test rig is used to investigate the factors affecting the broadband noise. The results show that the method can predict the magnitude and trend of each noise component of the fan without requiring a lot of computational and time costs, and has a good value for engineering use.

1 RESEARCH METHOD AND MODEL

Fast and efficient flow phase is one of the important indexes of fan aerodynamic and acoustic design, using the analytical method is suitable. While the calculation precision of the given analytical method is limited, but it can rapidly provide design personnel with general design idea regarding determination of design direction with the provision of reasonable adjustments.

1.1 Theory of sound propagation in flowing ducts

Aircraft engine fan mechanical components are typical of instream impeller machinery. A complete analysis of the acoustic field in the ducts of the turbomachinery needs to take into account the effects of airflow, velocity gradient, temperature gradient, etc. on the propagation and attenuation of acoustic waves. Also the acoustic effects of convection, refraction and scattering generated by the airflow in the ducts should be considered. However, if all of these factors are taken into account, research complexity will enhance exponentially. In order to integrate noise calculations into industrial systems, a simplification of the secondary issues is required. Therefore, for aircraft engine flow ducts, the fundamental problem of sound propagation in hard-walled circular as well as annular ducts is discussed.

The basic assumptions of the theoretical acoustic modelling of circular/annular ducts are as follows (M.E. Goldstein,1976):

(1) Incompressible medium, isentropic flow, subsonic flow, and temperature gradients are neglected;

(2) Axial mean velocity distribution and circumferential mean velocity distribution and the shape of the pipe cross-section remain constant in the axial direction;

(3) The flow has no radial velocity distribution;

(4) Both circumferential and axial flow rates do not change with time;

(5) The temperature and density of the medium are constant in space and time.

Based on the above assumptions, the equation of acoustic wave propagation in a circular/annular duct in a cylindrical coordinate system can be written as:

$$\frac{1}{c_0^2}\left(\frac{D}{Dt}\right)^2 p - \Delta p = 0 \tag{1}$$

In the above equation: p is the sound pressure; $\frac{D}{Dt}$ is the sound velocity; Δ is the current derivative in the cylindrical coordinate system; is the Δ Laplace operator in the cylindrical coordinate system.

For an acoustic field inside a circular/annular hard-walled duct, the solution of the acoustic wave equation is a linear superposition of different acoustic modal waves:

$$p(x,r,\theta) = \sum_{m=-\infty}^{\infty}\sum_{n=0}^{\infty}\left(A_{mn}^{+}e^{-\mathrm{i}k_{mn}^{+}x} + A_{mn}^{-}e^{-\mathrm{i}k_{mn}^{-}x}\right)\Psi_m(\kappa_{mn}r)e^{im\theta} \tag{2}$$

$$\Psi_m(\kappa_{mn}r) = B\cdot J_m(\kappa_{mn}r) + C\cdot Y_m(\kappa_{mn}r) \tag{3}$$

Where: m, n are the circumferential and radial modal orders, respectively; A is the acoustic modal amplitude; k is the axial wave number; x, r, θ is the axial, radial, and circumferential coordinates in the cylindrical coordinate system; Ψ, κ are the modal characteristic function and modal characteristic value of the cylindrical duct, respectively; J, Y are the Type I and Type II Bessel functions, respectively; B, C are the coefficients, which can be derived by dichotomisation (WANG,L.F,2017); $+, -$ and are the direction of the air flow direction and the reverse flow direction.

When the axial wave number is real, the acoustic modal wave propagates along the duct without attenuation, while when the axial wave number is imaginary, the amplitude of the acoustic modal wave shows an exponential decay along the duct. These two phenomena are called "cut-on" and "cut-off" phenomena of acoustic modal wave. The critical frequencies of the cut-on and cut-off states of acoustic modal waves are (QIAO,W.Y.,2010):

$$f = \frac{\kappa_{mn} \cdot \sqrt{1 - Mx^2}}{2\pi R_D} \cdot c_0 \tag{4}$$

Where: R_D is the casing radius; Mx is the mean airflow axial Mach number.

The sound power corresponding to different modes can be calculated from the amplitude of the acoustic modes in the duct (WANG,L.F,2017):

$$\wp_{mn}^{\pm} = \mp \frac{\pi(R_D^2 - R_H^2)}{\rho_0} \cdot \frac{(1 - Mx^2)^2 \omega \cdot \varepsilon_{mn}}{[\omega \pm Mx \cdot c_0 \cdot \varepsilon_{mn}]^2} \cdot [A_{mn}^{\pm} \cdot A_{mn}^{\pm *}] \tag{5}$$

$$\varepsilon_{mn} = \sqrt{(\frac{\omega}{c_0})^2 - (1 - Mx^2)\kappa_{mn}^2} \tag{6}$$

where: R_H is the hub radius; ρ_0 is the mean gas density; ω is the angular frequency.

From Eq. (5), it can be seen that the key to solving for the sound power in the pipe is to solve for the modal amplitude.

1.2 Fast calculation method for fan turbulence broadband noise

Unlike fan rotor-static interference monophonic noise, the sound source of fan turbulent broadband noise mainly comes from the interference effect of rotor-generated turbulence with the downstream static sub-blade. Therefore, two points need to be taken into account to establish a fan turbulence broadband noise prediction model: (1) simulate the turbulence generated by the rotor blades;(2) simulate the interfering effect of the turbulence with the downstream static sub-blade and compute the transient pressure on the surface of the static blade. Notice the fan needs time effectiveness, quick response in the design phase and the calculation of unsteady blade surface pressure without using a two dimensional cascade line unsteady theory, but at the same time employing a more direct and efficient Sear function(Sears,W.R,1941).

The acoustic power in the fan duct ζ_{mn} is calculated as(WANG L F,2017; TONG H et al,2020):

$$\zeta_{mn}(\omega) = \frac{\pi(r_D^2 - r_H^2)}{\rho U} \cdot \frac{\mp Ma^2(1 - Ma^2)^2(\omega / U)k_{mn}(\omega)}{[\omega / v \pm Mak_{mn}(\omega)]^2} \cdot [A_{mn}(\omega) \cdot (A_{mn}(\omega))^*] \tag{7}$$

where m and n are the circumferential and radial modal orders of the annular duct, is the angular frequency, r_D and r_H are the casing radius and hub radius, ρ is the gas density, U is the duct flow velocity, M_a is the Mach number, v is the sound velocity, k is the axial wavenumber, and A is the acoustic modal amplitude at the corresponding frequency and mode state:

In the case only dipole noise source is considered, stator blade of A_{mn} modal amplitude modulus square can be written as:

$$\left|A_{mn}^{\pm}(\omega)\right|^2 = B \int_{r=r_H}^{r_D} \left|g_{mn}\right|^2 \quad \left|\sigma_{L,mn}(\omega)\right|^2 \quad l_r(\omega) dr \tag{8}$$

where B is the number of sound source blades and g_{mn} is the Green's function of the annular duct:

$$\left|g_{mn}\right| = \frac{1}{2\mathrm{i}} \frac{\psi_m(\kappa_{mn} r)}{k_{mn}\pi(r_D^2 - r_H^2)} \tag{9}$$

where Ψ_{mn} and κ_{mn} are the modal eigen-functions and eigen-values of the annular duct, respectively.

σ is the sound source of the corresponding frequency and mode:

$$\left|\sigma_{mn}(\omega)\right|^2 = \left|k_{\perp,mn} \cdot c \cdot \frac{1}{2}\rho W^2 C_L(\omega)\right|^2 \tag{10}$$

Where, c is the chord length of the blade, W is the average airflow velocity of the incoming flow, $k_\perp$ is the wave number in the vertical direction of the blade surface, and C_L is the unsteady load coefficient:

$$C_L^2(\omega) = 4\pi^2 \frac{\hat{w}\hat{w}^*(\omega)}{W^2} S^2(\omega) \tag{11}$$

$\hat{w}\hat{w}^*$ is the upwash velocity spectrum of the incoming flow, and the relationship between $\hat{w}\hat{w}^*$ and the turbulent spectrum Φ_{ww} of the incoming flow is:

$$\lim_{T\to\infty} \hat{w}\hat{w}^* = \frac{U}{\pi}\Phi_{ww} \tag{12}$$

For the prediction of fan broadband noise, the turbulence spectrum generally selects the Liepmann turbulence spectrum, and the specific expression of one-dimensional Liepmann turbulence spectrum is given here (Wohlbrandt A et al,2016):

$$\Phi_{ww}(k) = \frac{8\overline{w}^2 \Lambda}{\pi} \frac{(\Lambda k)^4}{[1+(\Lambda k)^2)]^3} \tag{13}$$

Where, $\overline{w}$ is the average upwash speed; Λ is the turbulence length scale, both of which can be expressed in terms of turbulent kinetic energy TKE and turbulent dissipation ϖ ,

$$\overline{w} = \sqrt{(2/3)TKE} \tag{14}$$

$$\Lambda \approx 10\sqrt{TKE}/\varpi \tag{15}$$

$S(\omega)$ is the Sear function (Sears et al,1941):

$$S(\omega) = \frac{1}{\sqrt{1+4\pi\dfrac{\omega}{c\cdot W}}} \tag{16}$$

l_r is the radial correlation function (GUERIN S et al,2019):

$$l_r(\omega) = \overline{\Lambda}\frac{8}{3}\left[\frac{\Gamma(1/3)}{\Gamma(5/6)}\right]^2 \frac{z^2}{\sqrt{1+z^2}(3+8z^2)} \tag{17}$$

$$z = St/St_0 \tag{18}$$

$$St = \omega\overline{\Lambda}/W \tag{19}$$

$$St_0 = \sqrt{\pi}\,\Gamma(5/6)/\Gamma(1/3) \tag{20}$$

Where $\overline{\Lambda}$ is the circumferentially averaged turbulent length scale, and Γ is the Gamma function.

2 OBJECTIVE

In this paper, the Northwestern Polytechnical University single-stage axial fan aerodynamic noise test-bed (NPU-Fan) is selected as the calculation and analysis object.

2.1 NPU-Fan

The schematic and design parameters of the NPU-Fan are shown in Fig. 1 and Table 1, respectively. NPU-Fan is mainly composed of inlet bell mouth, inlet section, acoustic measurement section, fan/compressor test section and muffler exhaust pipe. A manual throttle cone is installed at the rear of the exhaust duct to control the working flow of the NPU-

Fan. The fan is powered by an 18.5 kW motor. In order to improve the noise measurement accuracy, the inlet section of the NPU-Fan is installed in a semi-anechoic chamber.

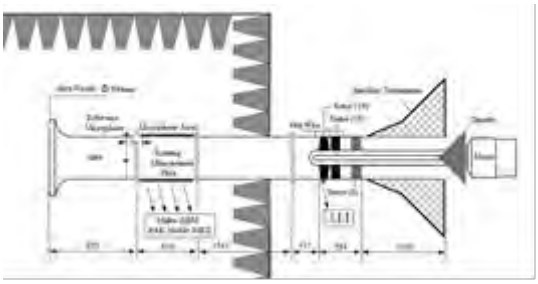

(a) Schematic diagram of the NPU-Fan structure

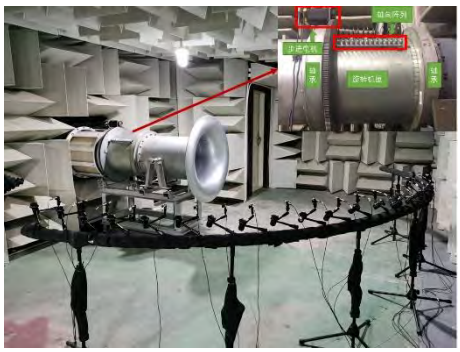

(b) Photo of the NPU-Fan

Fig. 1 Diagram of NPU-Fan

Table 1 NPU-Fan design parameter

Parameter	Value
Rotor blade number	19
Stator blade number	18
Shroud diameter（m）	0.5
Hub diameter（m）	0.285
Massflow（kg/s）	6.38
Design speed（r/min）	3000
Total pressure ratio	1.02
Airfoil shape	NACA-65

2.2 Calculation Settings

In this paper, the NPU-Fan is modelled to calculate the flow field for rotor speeds from 1100 r/min to 3000 r/min using the RANS method. Figure 2(a) shows the structure diagram of steady calculation domain of single-stage fan. In order to ensure the consistency with the experiment, a semicircular inlet cone is added in front of the rotor hub. The inlet boundary condition of the calculation domain is the total pressure boundary condition: 97700Pa, the mean static pressure boundary condition at the outlet, the non-slip boundary condition at the solid wall and the rotating periodic boundary condition at the circumferential direction. In the calculation, the governing equations are solved by the finite volume method, the second order difference scheme is used in space, the second order backward Euler scheme is used in time, and the SST(Shear-Stress Transport) turbulence model based on $k-\omega$ is selected. Figure 2(b) is the size diagram of steady calculation domain of single-stage fan. The blade tip clearance of rotor is 0.6mm, the chord length of stator blade is about 90mm, the axial length of the whole calculation domain is 900mm, the dotted line position is the rotor-stator interface, and the total pressure mixing interface is adopted in steady calculation of single-stage fan.

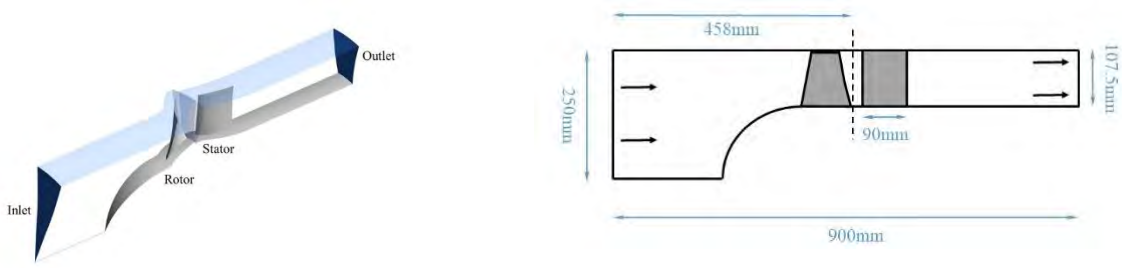

(a) Diagram of CFD computational domain **(b) Size of CFD computational domain**

Fig. 2 Diagram of NPU-Fan steady computational domain

2.3 Grid setting

Figure 3 shows a schematic of the NPU-Fan rotor/stator blade surface mesh. In order to ensure the independence of the grid to the numerical calculation, a total of 4 sets of grids are divided, with grid numbers of 2.1 million, 3.8 million, 6.1 million and 7.9 million respectively. The dimensionless grid scale of most of the blade surface of the four sets of grids is y+1, which meets the grid requirements of SST calculation.

(a) Mesh of rotor blades **(a) Mesh of stator blades**

Fig. 3 Schematic of NPU-Fan rotor/stator blade surface mesh

Figure 4 shows the results of NPU-Fan grid independence study verification. Figure 4(a) shows the circumferential average turbulent kinetic energy distribution of stator incoming flow under different grid numbers, and Figure 4(b) shows the circumferential average turbulent length scale distribution of stator incoming flow under different grid numbers. It can be seen from Fig. 4 that the distribution law of the turbulent information of the incoming flow calculated through the four sets of grids is approximately the same. In comparison, the grid amount of 2.1 million is slightly insufficient. The calculation of the circumferential average turbulent kinetic energy is reduced by about 0.7 J/kg at most in the region below 40% spanwise height, and the calculation of the circumferential average turbulent length scale is reduced by about 2 mm at most in the region above 60% spanwise height. Generally, when the number of grids is more than 3.8 million, the change of grid number will not produce obvious change on the calculation results of turbulence information. Assuming that the maximum difference of turbulent kinetic energy is less than 10%, the maximum difference of velocity spectrum of incoming turbulent flow is less than 10%, and the absolute magnitude difference of sound power of broadband noise is less than $10lg(1.1)$ 0.41dB, which is completely negligible for broadband noise prediction. A grid size of 6.1 million was selected for further calculations and analysis after weighing the accuracy and available computing resources.

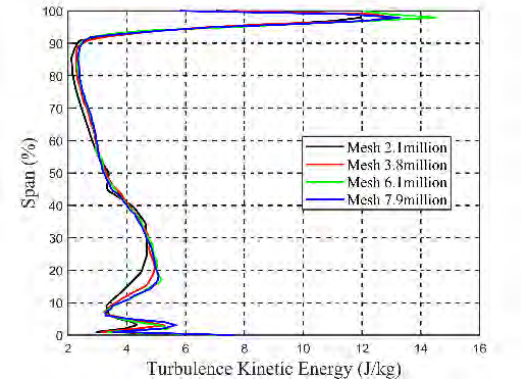

(a) Circumferential average TKE along span

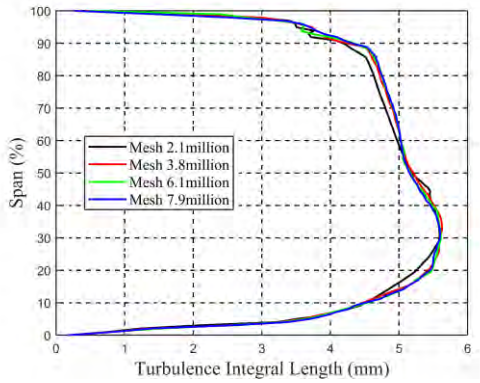

(b) Circumferential average Λ along span

Fig. 4 NPU-Fan grid independence verification

3 CALCULATION RESULTS AND ANALYSIS

3.1 Model validation

In order to verify the reliability of the fast prediction method of turbomachinery duct broadband noise, the international open standard (ISO) experiment was used to check it. As shown in Fig. 5, Posson and Roger designed an annular cascade test rig(Posson H et al,1907), installed in an anechoic chamber at the Ecole Centrale de Lyon (background noise: 20 dBA, cut-off frequency: 100 Hz). In order to remove the rotor self-noise as an interference term and to facilitate a more direct study of turbulence-blade interference noise, the device did not use the rotor to generate turbulent wake, rather the turbulence grill was used at the nozzle to generate turbulence at different scales.

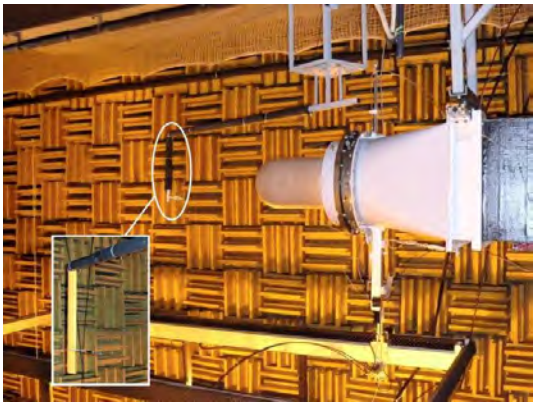

(a) External environment

(b) Overall structure

Fig.5 The annular cascade test bench physical diagram

Fig.6 Geometric sketch shows the annular cascade. Over the course of experiment, the two groups of Cascade: A set of blades for 49 (Cascade1), another group of leaf number is 98 (Cascade 2).Two sets of blade Installation Angle is 16.7 °, chord length of 25 mm.

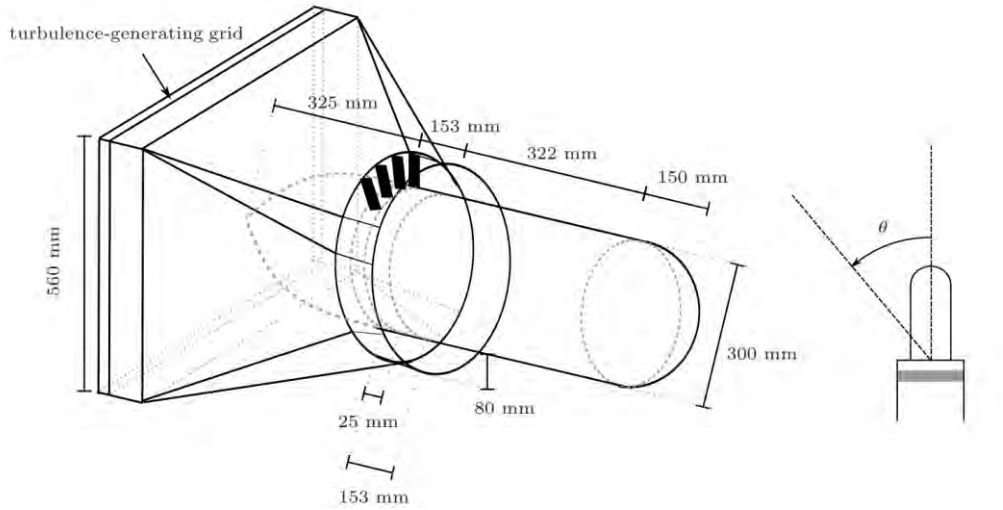

Fig.6 the annular cascade geometry diagram

Experiments also adopted two groups of turbulence grids, used to generate different intensity and scale of turbulence. Two groups of turbulence grids providing diverse turbulence intensity of about 3% respectively (Gird 1, table 2) and 5.5% (Gird 2, table 3). The turbulence information obtained from the experiments in Tables 2-2 and 2-3 is used as inputs, using fan turbulence broadband noise fast calculation method to calculate the annular cascade noise level of the de Lyon central university of technology.

Table 2 Turbulence information generated by Gird 1

r/R_m	0.84	0.87	0.895	0.92	0.95	0.975	1.0
Tu	4.63	4.07	3.87	3.78	3.68	3.61	3.63
Λ(mm)	23	21	20.5	19	17.5	17	17

(续)

r/R_m	1.02	1.06	1.08	1.11	1.13	1.16	1.18
Tu	3.6	3.53	3.49	3.36	3.18	3.14	3.22
Λ(mm)	16	16	16	15.5	15	16	17

Table 3 Turbulence information generated by Gird 2

r/R_m	0.84	0.87	0.895	0.92	0.95	0.975	1.0
Tu	6.87	6.33	6.06	6.03	6.20	6.09	6.05
Λ(mm)	23	23	22	20	20	19	19

(续)

r/R_m	1.02	1.06	1.08	1.11	1.13	1.16	1.18
Tu	6.00	5.96	5.97	5.86	5.71	5.31	5.46
Λ(mm)	19	19	19	19	17	19	19

Fig. 7 give a comparison between the acoustics computational results of the various methods and the experimental results of annular cascade, used in de Lyon Central University as the study object. It can be seen that the results obtained by the fast calculation method for fan turbulence broadband noise in this thesis are in agreement with the trend of Posson's calculations (Posson H et al,1907) and Hanson's calculations (Hanson DB et al,1998). For the frequency range below 1 kHz, all three broadband noise prediction methods are sensitive to the "cut-off" and "cut-through" states of the acoustic modes. This is due to the fact that in the low frequency range there are very few acoustic modes that are in the "cut-off" state, and whenever a new acoustic mode starts to "cut-off", it introduces new energy at the critical frequency, which has a

significant effect in the low frequency range. This phenomenon decreases with increasing frequency, and it can be seen that in the frequency range above 3 kHz, the noise spectrum has basically levelled off.

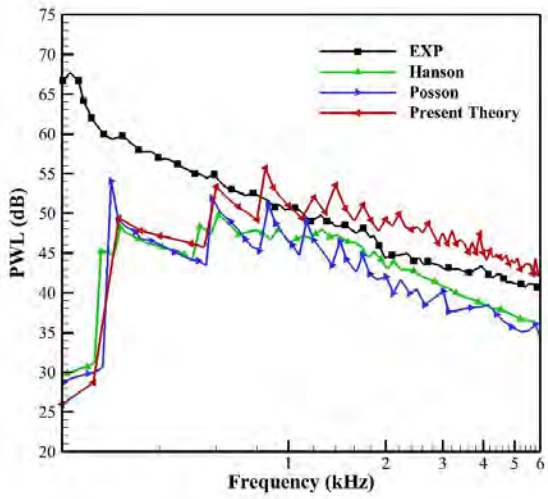

（a）Cascade 1 & Gird 1

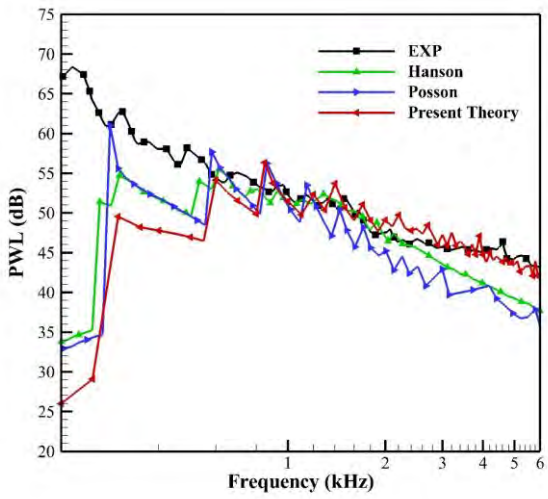

（b）Cascade 1 & Gird 2

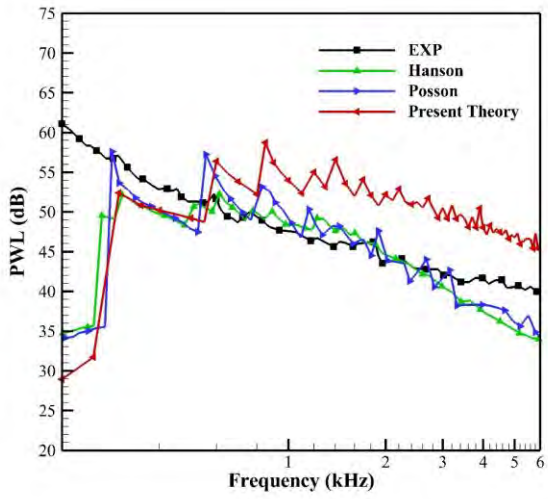

（c）Cascade 2 & Gird 1

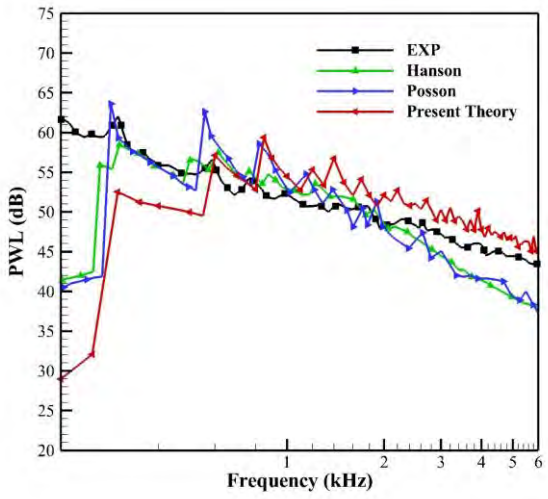

（d）Cascade 2 & Gird 2

Fig. 7 Annular cascade prediction results and the experimental results of contrast

As can be seen from Fig. 7, the results obtained by the fast calculation method of fan turbulence broadband noise in this thesis are overall larger compared to those of Posson and Hanson, and the calculation results in Fig. 7(a) and (c) are also significantly larger relative to the experimental results, which may be analysed as a result of the following two reasons:

(1) This paper establishes that fan turbulence broadband noise fast calculation method used in the blade response function is the Sear function, the advantage of this approach is to solve the unsteady blade surface without requiring complicated iteration, fast computational speed, whereas the disadvantage is that the form of the Sear function is simple and ignore the cascade effect. Comparison of Figures 7(a) and (b), Figures 7(c) and (d) shows that in the case of constant free stream turbulence, the larger the number of blades the greater the error in the results. So that the stronger the cascade effect, the easier it is to make the mistake in calculation.

(2) The turbulence spectrum used in the fast calculation method of fan turbulence broadband noise established in this thesis is a 1-D Liepmann turbulence spectrum. The turbulence spectrum in the real turbulence - cascade interference process should be a three-dimensional turbulence spectrum, and part of the turbulence energy in the circumferential and radial directions will not act on the blades, so the 1-D turbulence spectrum overestimates the energy of the generated noise compared to the three-dimensional turbulence spectrum.

Overall, although the rapid broadband noise prediction method established will slightly overestimate the noise level, the trend of the results is accurate. The method requires very little resources and time for calculation. Considering the calculation accuracy and calculation time together, the method possesses good calculation accuracy as well as good timeliness.

3.2 Aerodynamics Results of NPU-Fan

The total pressure ratio characteristics of NPU-Fan at 3000rpm, 2700rpm and 2400rpm were calculated. It can be seen from Figure 6 that the largest discrepancy between calculation and experiment is about 0.1% at 3000rpm and about 0.04% at 2400rpm. The experimental and computational results have a difference of 0.06kg/s at the surge boundary, which is about 1.44%. It can also be seen from Figure 6 that the results of medium massflow rate and large massflow rate conditions cannot be obtained in the experiment. The reason may be related to the loss along the outlet pipe and the structure of the throttle valve, which limits the measurement range of the fan experiment.

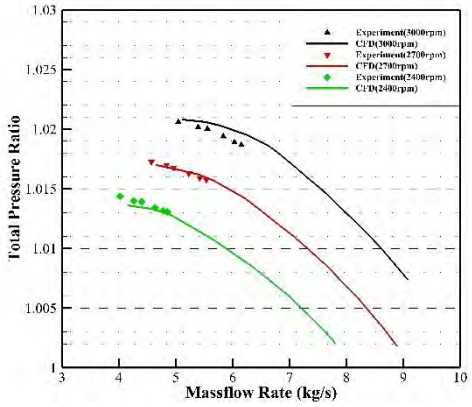

Fig. 2 Comparison of numerical and experimental results of NPU-Fan aerodynamic performance

In order to quantitatively correlate the relationship between the stator incoming turbulence information and the fan operating state, the changes in the distribution of the NPU fan stator incoming turbulence information are respectively shown in Fig. 7 and Fig. 8 for the 3000 rpm and 2700 rpm operating states. It can be seen from Fig.7(a) and Fig.8(a) that the total level of circumferentially averaged turbulent kinetic energy of the NPU fan shows a decrease followed by an increase as the massflow rate increases at two different rotor speeds. Meanwhile, the region of high turbulent kinetic energy is mainly concentrated in the region above 90 % and below 10 % of the span height of the blade. Therefore, for the NPU-Fan, the rotor tip leakage flow and the boundary layer turbulence are the main contributors to the average turbulent kinetic energy of the stator incoming flow. As can be seen from Fig.7(b) and Fig.8(b), the circumferentially averaged turbulence length scales of the NPU fan at two different rotor speeds show a significant increase with decreasing mass flow rate. This means that the circumferentially averaged length scale of the turbulence is highly correlated with the massflow rate.

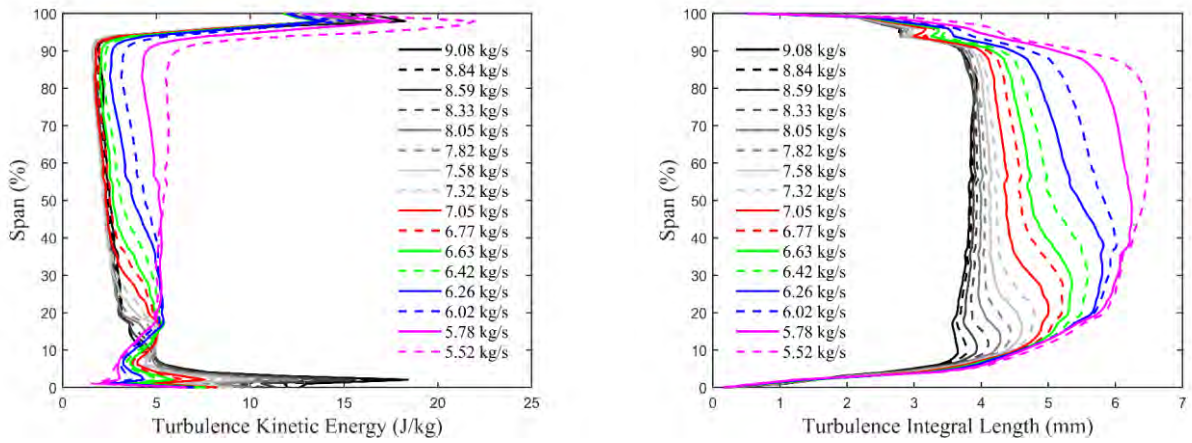

(a) the circumferential average turbulent kinetic energy

(b) the circumferential average turbulence length scale

Fig. 7 Variation of turbulence information of NPU-Fan stator incoming flow with flow rate at 3000 r/min.

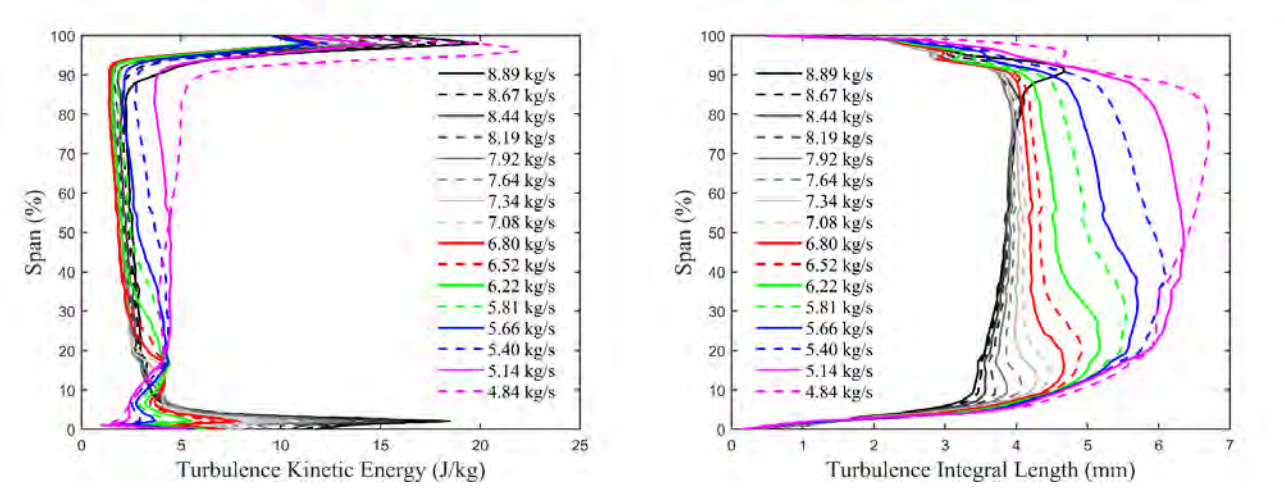

(a) the circumferential average turbulent kinetic energy

(b) the circumferential average turbulence length scale

Fig. 8 Variation of turbulence information of NPU-Fan stator incoming flow with flow rate at 2700r/min.

From Fig. 7 and Fig. 8, it can be seen that as the massflow rate increases, the turbulent kinetic energy in the position near the hub (about 0% to 15% spread) gradually decreases, while the turbulent kinetic energy in other positions gradually increases. In order to explain this phenomenon, Fig.9 shows the structure of the flow field at the root of the rotor for three different flow rates at 3000 rpm. The main cause of this phenomenon is the induced horseshoe vortex at the leading edge of the rotor root, as shown in Fig.9. At the same time, the horseshoe vortices induced at the leading edge of the rotor root are mainly concentrated at the root of the rotor channel under high massflow rate.

As the flow rate decreases, the pressure-side branch of the horseshoe vortex is shifted towards the suction-side of the rotor, and the suction-side branch of the horseshoe vortex is also more likely to move towards the middle of the blade. It is obvious from Fig. 9(c) that when the massflow rate is 5.52 kg/s, the horseshoe vortex pressure surface branch and the suction surface branch converge and develop close to the suction surface of the rotor while moving towards the middle of the blade. Thus, for fan components, the induction of horseshoe vortices at the leading edge of the rotor root can have a significant effect on the distribution of turbulent kinetic energy along the span heights.

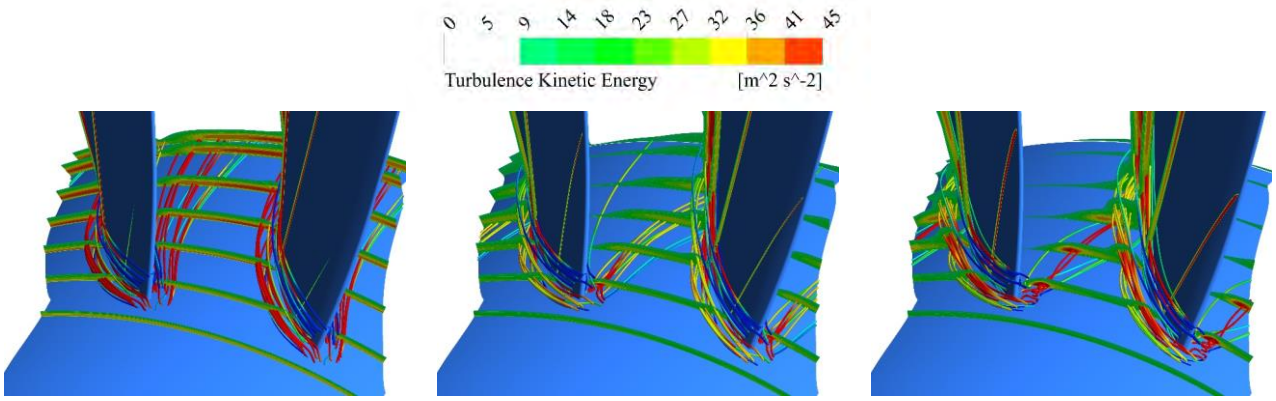

（a）9.08kg/s **（b）6.38kg/s** **（c）5.52kg/s**

Fig. 9 Variation of flow field at the root of NPU-Fan rotor with flow rate at 3000r/min

The fan characteristics at 80% to 100% rotor speed are given by the RANS method, and a simpler and more intuitive method is used here to represent the fan aerodynamic characteristics. Fig. 10 shows the aerodynamic performance of the NPU-Fan for rotor speeds from 1100 rpm to 3000 rpm. In the graph, the horizontal coordinate is the massflow rate, the vertical coordinate is the total pressure ratio, and the background colouring represents the fan efficiency. The white part indicates the working area where the NPU-Fan does not work properly. Fig. 10 shows the total pressure ratio and efficiency characteristics of the fan, so that the operating state of the fan can be selected according to the needs.

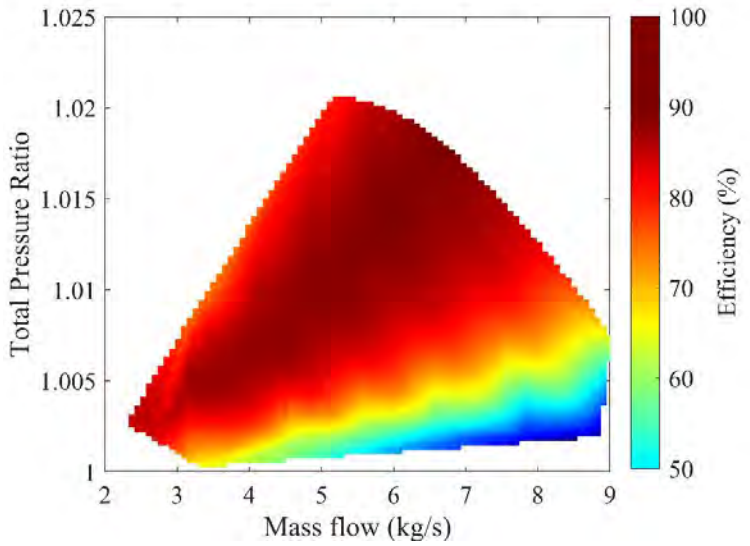

Figure10 NPU - Fan aerodynamic performance cloud

3.3 Acoustic Results of NPU-Fan

A comparison between the predicted and experimental results of the NPU-Fan inlet broadband noise is given in Fig. 11. In the Fig.11, the black line is the broadband noise sound power calculated by the two-point microphone method (XV,K.B.,2018).The red line is the result of the broadband noise that has been filtered out by the Rowless filter for tone noise and other interference. The green line (Method 1) is the broadband noise result calculated by the fan broadband fast calculation method described in this paper, and the blue line (Method 2) is the broadband noise result obtained by using the quasi-3D fan noise calculation method(Tong, H. et al, 2021).

As can be seen in Fig. 11, in the frequency range below 600 Hz, the results obtained using the two different broadband noise calculation methods are on the low side. This phenomenon suggests that the fan rotor/stator interaction broadband noise is not the dominant contributor in this frequency range. At frequencies above 600 Hz, the fan rotor/stator interaction broadband noise becomes the most dominant contributor to the fan broadband noise. In addition, consistent with the phenomenon shown in Fig. 7, the results obtained by the fast fan broadband noise calculation method overpredict the broadband noise in the mid-and high-frequency ranges, whereas the results obtained by the quasi-3D fan broadband noise calculation method are much more accurate (with a peak error of about 2.77 dB, which is less than 3 dB).

In reference (WANG, L. F.,2017), Dr Wang Liangfeng also suffered from over-prediction of broadband noise at mid- and high-frequencies when using the Gliebe model(Gliebe, P., 2002). Therefore, the authors speculate that the most important reason for this phenomenon is the result of an oversimplified response function in the model, which does not take into account the cascade effect. In addition, compared to the 3D turbulence spectrum, part of the turbulence energy in the circumferential and radial directions of the 1-D turbulence spectrum and the 2-D turbulence spectrum does not act on the blade sounding, and they overestimate the turbulence energy that generates the noise.

The authors used a program running platform configured with a CPU of i7-11700K (8 cores) and 128 GB of RAM (frequency: 2400 MHz). In the case of this example (shown in Fig. 11), it takes about 1 to 2 core-hours using the turbulent broadband fast calculation method described in this paper, and about 200 to 300 core-hours using the quasi-3D fan noise calculation method (Tong, H.et al, 2021). The authors have incorporated a parallelism strategy in the programming, so that with 8 cores in parallel, the turbulence broadband fast prediction method described in this paper takes about 7 to 15 minutes, and the quasi-3D fan noise calculation method (Tong, H.et al, 2021) takes about 1500 to 2300 minutes. Overall, the fan broadband noise fast prediction method described in this paper has a relatively low accuracy, but the computational speed is extremely fast, which is very important.

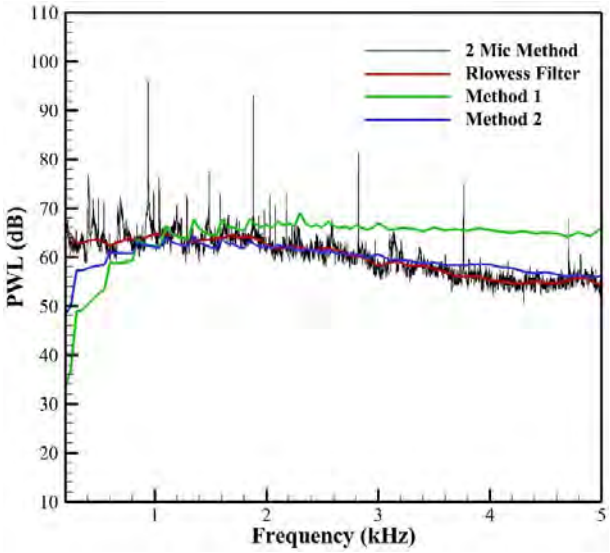

Figure 11 NPU - Fan forward noise sound power contrast (3000 r/min, 5.8 kg/s)

The variation of NPU-Fan forward noise sound power with massflow rate at 3000 rpm and 2700 rpm speeds is given in Fig. 12. From the figure, it can be seen that under two different rotor speed conditions, the broadband noise spectra all show the characteristics of the turbulent broadband noise component shifting from mid- and high-frequency to low-frequency as the flow rate decreases .Comparing Fig. 7(b) and Fig. 8(b), it can be seen that the circumferentially averaged turbulence length scale increases significantly as the flow rate decreases, due to the fact that small-scale turbulence is associated with high-frequency noise and large-scale turbulence is associated with low-frequency noise. Therefore, the migration phenomenon of turbulent broadband noise energy in Fig.12 is caused by the change of turbulence length scale due to the change of flow rate.

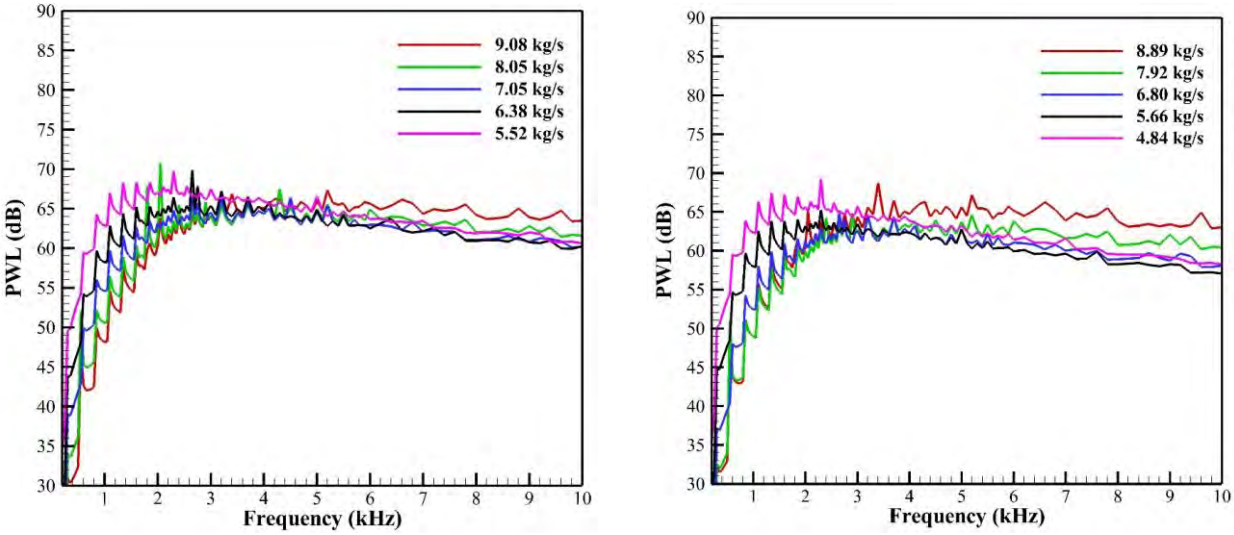

（a）3000 r/min **（b）2700 r/min**

Fig. 12 Variation of NPU-Fan forward noise sound power with flow rate

As can also be seen from Fig.12, an increase in fan massflow increases the noise level of the fan. If the fan operating range is close to the unstable operating line, the noise level will also increase significantly.Comparing Fig. 7(a), Fig. 8(a) and Fig. 9, it can be seen that when the fan is operating at a low massflow rate, the fan rotor blades induce severe airflow separation and secondary flow at the tip of the blades, which increases the intensity of the incoming turbulence at the stator, and the turbulence interferes with the downstream stator generating a strong broadband noise.

The Overall Sound Power Level (OAPWL) is defined as Equation (21). The frequency integration range is selected from 200 Hz to 10000 Hz which is commonly used for Aircraft engine aerodynamic noise.

$$OASPL = 10 \cdot \lg \cdot \int_{Frequency_{low}}^{Frequency_{high}} Power(f)df \tag{21}$$

At a rotor speed of 3000 rpm, compared to the design condition (6.38 kg/s), the noise increases by about 0.80791 dB in total sound power level at a flow rate of 9.08 kg/s, and by about 1.27 dB in total sound power level at a flow rate of 5.52 kg/s. Figure 12(a) shows that when the frequency is greater than 5 kHz, compared with the design condition, the sound power level increases by about 2~4 dB at a flow rate of 9.08 kg/s, and the sound power level increases by about 0.5~1 dB at a flow rate of 5.52 kg/s. In the frequency range greater than 3 kHz, the sound power level increases by about 2 to 5 dB for a flow rate of 5.52 kg/s.

The cloud plot of inlet sound power characteristics of NPU-Fan is given in Fig. 13. From Fig. 13, it can be seen that the broadband noise of the NPU-Fan basically tends to increase with increasing massflow rate as well as increasing speed. In addition, comparing Fig. 13 with Fig. 10, it can be seen that for the NPU-Fan, when the operating range of the fan is at a high aerodynamic efficiency, the broadband noise level of the fan is at a lower level. When the operating range of the fan is near the instability boundary, although the operating flow rate is small, the turbulent kinetic energy of the stator incoming flow is still at a very high level, which leads to a significant increase in the overall broadband noise of the fan. When the operating range of the fan is in the high-flow operating range, on the one hand, the increase of the stator flow velocity leads to the enhancement of the incoming turbulent kinetic energy, and on the other hand, the increase of the Mach number of the inlet duct leads to a high number of modes of the cut-off pass. As a result, the increase in flow rate also leads to the enhancement of the broadband noise of fan. Some basic rules can be obtained from this study: the overall level of the fan broadband noise depends on the level of the turbulent kinetic energy of the stator blades, and the optimal operating range of the fan is near the design conditions, and the aerodynamic and acoustic optimal operating points of the fan are the same.

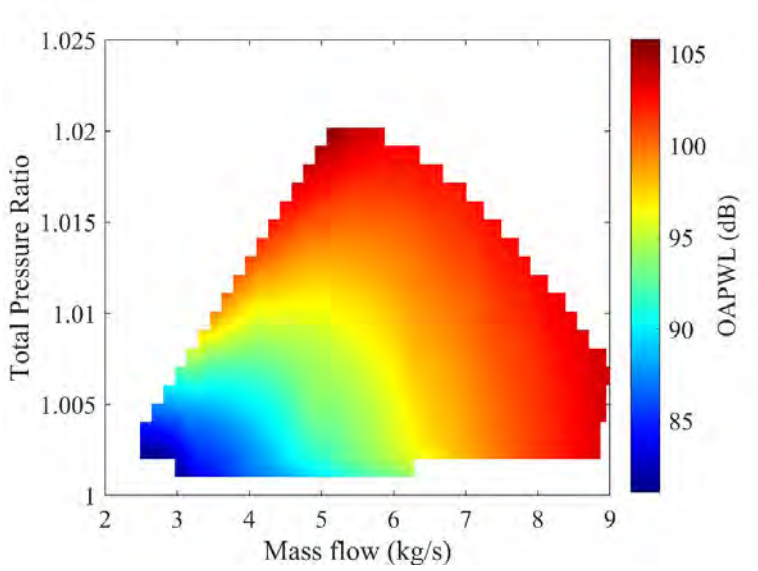

Figure 13 NPU-Fan Acoustic Characteristics Cloud

4 CONCLUSION

In this paper, firstly, based on the theory of sound propagation in the flow duct, combined with the blade response function, a fast calculation method of fan rotor-stator interaction broadband noise is established, and then the method is verified; Then a single-stage low-speed axial fan was taken as the research object, and the regularity study of fan blade exhaust turbulence and broadband noise was carried out by using the RANS method and the broadband noise fast calculation method.

The main conclusions are as follows:

（1）The fast calculation method of fan turbulence broadband noise established in this paper is validated by using the experimental bench of annular vane grating at the University of Lyon, France. The calculation results have the same trend compared with the results of foreign scholars, but the magnitude is more on the large side. Taking a single-stage low-speed axial fan as the research object, it is clear that the reason for this phenomenon after comparing with the results of the quasi-three-dimensional broadband noise calculation method, is that the response function of the impeller effect is not taken into account, and the one-dimensional turbulence spectra of the sound-generating energy are overestimated. Considering the calculation accuracy and calculation time, the fast method of fan turbulence broadband noise calculation has better

calculation accuracy and good timeliness time-effectiveness, which is more suitable for the broadband noise calculation and evaluation in the design stage of fan turbulence.

（2）It is found that the horseshoe vortex induced by the leading edge of the rotor root has an obvious effect on the distribution of turbulent kinetic energy along the span. Specifically, the horseshoe vortex induced by the leading edge of the rotor root is mainly concentrated in the rotor channel root under the high flow rate condition. With the decrease of the flow rate, the pressure side branch of the horseshoe vortex will deflect to the rotor suction side faster, and the suction side branch of the horseshoe vortex will move more easily to the middle of the blade.

（3）It is found that the increase of the working flow rate will significantly increase the forward noise of the fan. However, when the working range of the fan is near the unstable operating line, the rotor is in a serious bad working condition, resulting in serious flow separation and tip secondary flow, which induces significant turbulence intensity, thus leading to high noise level.

In a nutshell, the fast prediction method of the broadband noise of the single-stage fan proposed in this paper has the characteristics of obtaining fast and accurate results, and can quickly obtain the acoustic characteristics of the single-stage fan in the broadband noise prediction stage, which is very suitable for engineering application.

Acknowledgements

The present work is supported by the National Natural Science Foundation of China (No. 52276038, 51936010 and51776174) and the National Science and Technology Major Project of China (No. 2017-Ⅱ-0008-0022).

References

[1] CHEN, H., YUAN, X. X., BI, L., et al (2023). Simulation of separated flow based on RANS/LES hybrid method. *Acta Aeronautica et Astronautica Sinica*, 44(2) pp.626310.

[2] Enghardt L (2019) Aeroacoustics Research in Europe: The CEAS-ASC report on 2017 highlights. *Journal of Sound and Vibration* 450: 175–198.

[3] Envia E (2001) Fan noise reduction - an overview. *39th Aerospace Sciences Meeting and Exhibit*.

[4] Gliebe, P., (2002). Fan Broadband Self Noise Prediction Model. 8th AIAA/CEAS Aeroacoustics Conference & Exhibit, AIAA ,2002-2490.

[5] Guerin S, Kissner CA, Kajasa B, et al. (2019) Noise prediction of the ACAT1 fan with a rans-informed analytical method: Success and Challenge. *25th AIAA/CEAS Aeroacoustics Conference*.

[6] Hanson D and Horan K (1998) Turbulence/cascade interaction - spectra of inflow, Cascade Response, and noise. *4th AIAA/CEAS Aeroacoustics Conference*.

[7] HUGHES, C. (2013). NASA collaborative research on the ultra high bypass engine cycle and potential benefits for noise, performance, and emissions. *NASA Technical Mem-orandum,* TM-2013-216345.

[8] Ju H (2016) Effects of vane sweep on fan-wake/outlet-guide-vane interaction broadband noise. *22nd AIAA/CEAS Aeroacoustics Conference*.

[9] Ju H, Mani R, Vysohlid M, et al. (2015) Investigation of fan-wake/outlet-guide-vane interaction broadband noise. *AIAA Journal* 53(12): 3534–3550.

[10] M. E. Goldstein.(1976). Aeroacoustics.McGRAW-HILL International Book Company.

[11] OWENS, R. (1979). Energy efficient engine: Propulsion system - aircraft integration evaluation. *NASA/CR,* 159488.

[12] Polacsek C, Clair V, Le Garrec T, et al. (2015) Numerical predictions of turbulence/cascade-interaction noise using computational aeroacoustics with a stochastic model. *AIAA Journal* 53(12): 3551–3566.

[13] Posson H and Roger M (2011) Experimental validation of a cascade response function for fan broadband noise predictions. *AIAA Journal* 49(9): 1907–1918.

[14] QIAO,W.Y.(2010). Aeroacoustics. Beihang University Press.

[15] SEARS WILLIAMR (1941) Some aspects of non-stationary airfoil theory and its practical application. *Journal of the Aeronautical Sciences* 8(3): 104–108.

[16] SHI, F. C., GAO, Z. X., TIAN, Y. Y., et al (2023). Large eddy simulation of ideally expanded supersonic jet noise. *Acta Aeronautica et Astronautica Sinica*, 44(2) pp.626266.

[17] Tong, F, Qiao W, Xu K, et al. (2018) On the study of wavy leading-edge vanes to achieve low fan interaction noise. *Journal of Sound and Vibration* 419: 200–226.

[18] TONG, H., DING, S., XIANG, X. S., et al (2021). Numerical study on tonal noise reduction of single axial fan with distributed wavy leading-edge stator. *Journal of Pro-pulsion Technology*, 42(10), pp.2237-2248.

[19] TONG,H., LI L., MAO L. Q. , et al (2020). Tonal noise reduction of a high-speed single axial fan with wavy leading-edge stator. *Acta Aeronautica et Astronautica Sinica*, 41(10), pp. 123565.

[20] TONG, H, LI L, WANG L, et al. (2021) Investigation of rotor–stator interaction broadband noise using a RANS-informed analytical method. *Chinese Journal of Aeronautics* 34(10): 53–66.

[21] WANG, L. F. (2017). *Experiment and numerical study on duct mode identification of fan noise*. Ph.D. Northwestern Polytechnical University.

[22] Wohlbrandt A, Hu N, Guérin S, et al. (2016) Analytical reconstruction of isotropic turbulence spectra based on the Gaussian transform. *Computers & Fluids* 132: 46–50.
[23] XV,K.B.(2018). Numerical and Experimental Study on Turbo-machinery Ducted Mode. Ph.D. Northwestern Polytechnical University.
[24] YAN, Q., XUE, D. W., GAO, X., et al (2022). Acoustic perfor-mance experimental technology of aircraft nacelle acous-tic liner. *Acta Aeronautica et Astronautica Sinica*, 43(6): pp.526810.